Available online at www.sciencedirect.com
SCIENCE DIRECT
Journal of Catalysis 234 (2005) 300–307
JOURNAL OF CATALYSIS
www.elsevier.com/locate/jcat

The active and reusable catalysts in the benzylation of anisole derived from a heteropoly acid

Kazu Okumura *, Katsuhiko Yamashita, Miho Hirano, Miki Niwa

Department of Materials Science, Faculty of Engineering, Tottori University, Koyama-cho, Tottori 680-8552, Japan

Received 23 March 2005; revised 25 June 2005; accepted 28 June 2005

Available online 10 August 2005

Abstract

Benzylation of anisole with benzyl alcohol was carried out with H_3PO_4–WO_3–Nb_2O_5-derived catalysts. The catalytic performance depended significantly on the calcination temperature. The catalyst calcined at 573–723 K exhibited low activity and poor reusability, and the formation of heteropoly acid (HPA), which is similar to 12-tungstophosphoric acid, was identified by infrared (IR) and X-ray diffraction (XRD) measurements. The catalysts calcined above 823 K were in essence inactive in the reaction due to the formation of crystalline WO_3 that originated from HPA. In contrast, optimum activity was realized for the catalyst calcined at 773 K, which could be readily reused after filtration. The acid property of H_3PO_4–WO_3–Nb_2O_5 was measured by means of NH_3 TPD and the IR spectra of adsorbed pyridine. An enhancement of weak acid sites was observed for the catalyst calcined at 773 K, accompanied by the simultaneous reduction in the acidity due to HPA. The Brønsted acid sites were dominant in H_3PO_4–WO_3–Nb_2O_5 calcined at 773 K. The partially decomposed HPA, which maintained the same local symmetry around W atoms as HPA, was observed with W-L_3 edge EXAFS as well as W-L_1 edge XANES. From these data, the active and insoluble species obtained by the calcination of H_3PO_4–WO_3–Nb_2O_5 at 773 K was ascribed to the intermediate species of HPA formed in the decomposition process.

Keywords: Friedel–Crafts alkylation; Heteropoly acid; Niobium oxide; NH_3 TPD; XAFS

1. Introduction

When using solid acid catalysts in organic synthesis, both high activity and reusability of the catalyst is desirable in view of the separation of products and the recycling of catalysts. Heteropoly acids (HPAs) are promising materials with strong acidity; therefore, they are used as catalysts for various types of organic synthesis, including selective oxidation and acid-catalyzed organic reactions [1–4]. However, the high solubility of HPA in polar solvents hampers its application to liquid phase reactions. The difficulty has been overcome by the inclusion of HPA in the silica matrix [5,6], formation of acidic cesium salt ($Cs_{2.5}H_{0.5}PW_{12}O_{40}$) [7,8], and encapsulation of 12-molybdophosphoric acid or 12-tungstophosphoric acid (HPW) in the pores of Y-type zeolite [9,10]. Another drawback of HPA is its low thermal stability when applied to a high-temperature reaction, such as cracking of alkane. In the case of HPW, deactivation begins at a lower temperature in many catalytic reactions despite the stability of the Keggin structure up to 823 K [11].

In this paper, we report that partially decomposed HPA derived from ternary mixed oxides (H_3PO_4–WO_3–Nb_2O_5) exhibited excellent catalytic performance, with facile reusability as well as high activity in the benzylation of anisole using benzyl alcohol. This reaction is a type of Friedel–Crafts alkylation in which the alkyl group can be readily introduced on an aromatic ring. The Friedel–Crafts reaction using HPA catalysts has attracted considerable attention in recent years [3,4,12,13]. The reaction scheme used in the present study is as follows (1):

* Corresponding author. Fax: +81-857-31-5684.
E-mail address: okmr@chem.tottori-u.ac.jp (K. Okumura).

0021-9517/$ – see front matter
doi:10.1016/j.jcat.2005.06.033

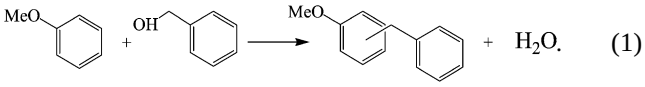

(1)

In this reaction, a side reaction occurs to form dibenzylether. The catalytic performance was related to the structural characterization, and the acid properties were measured by means of X-ray diffraction (XRD), infrared spectroscopy (IR), X-ray absorption near edge structure (XANES), extended X-ray absorption fine structure (EXAFS), and NH_3 temperature-programmed desorption (NH_3 TPD) methods to investigate the reason for the significant changes in catalytic performance at different calcination temperatures.

2. Experimental

2.1. Catalyst preparation

Niobium oxalate was prepared by dissolving 1.27 g of niobic acid (supplied by CBMM Co.) in an oxalic acid (Wako Co., 4.77 g) solution (100 ml) on a hot plate at 353 K. $(NH_4)_{10}W_{12}O_{41} \cdot 5H_2O$ (Wako Co., 1.69 g) was dissolved in deionized water (100 ml). The solution of niobium oxalate and $(NH_4)_{10}W_{12}O_{41}$ was mixed, and then 85% phosphoric acid (0.22 g) was added. The admixture solution was evaporated on the hot plate with continuous stirring. The obtained solid was calcined at 573–773 K for 3 h in air. The surface area of H_3PO_4–WO_3–Nb_2O_5 calcined at 773 K was found to be 58 $m^2\,g^{-1}$ by the BET method. The composition of the prepared H_3PO_4–WO_3–Nb_2O_5 was determined by ICP analysis after digestion with HF solution. As an experiment for comparison, montmorillonite-K10 clay modified with sulfuric acid was prepared as described previously [14]. Montmorillonite-K10 clay is known to have characteristics of Brønsted acid and a large specific surface area [15]. The acid treatment makes the surface of the montmorillonite-K10 clay acidic [16]. In the preparation, montmorillonite-K10 clay (supplied from Aldrich, Co., 0.25 g) was stirred in 50 ml of 30 wt% sulfuric acid for 2 h at 353 K, followed by filtering, washing, and calcination at 773 K in air.

2.2. Catalytic reaction

A total of 0.1 g of the catalyst was used for the benzylation of anisole. The pretreatment was carried out in an N_2 flow at 673 K for 1 h but at 573 K for the H_3PO_4–WO_3–Nb_2O_5 catalyst calcined at 573 K during the preparation (Fig. 3). The reaction was performed using 10 g of anisole and 0.675 g (6.25 mmol) of benzyl alcohol in an oil bath at 333–353 K under an N_2 atmosphere for 3 h. For recycling, the catalyst was separated by filtration, followed by washing with anisole. The catalyst was then used repeatedly for further reaction without pretreatment. The products were analyzed by gas chromatography (GC) (GC-2010, Shimadzu) equipped with a capillary column MDN-12 and FID detector. In the analysis, tridecane was used as an internal standard.

2.3. XRD measurement

The crystalline structure was analyzed by XRD in ambient conditions using a Rigaku Mini-flex plus X-ray diffractometer with CuK_α radiation.

2.4. IR measurement

Fourier transform IR measurement (Fig. 4) was carried out using the Spectrum One spectrometer (Perkin Elmer). Before the measurement, the sample was pressed to form pellets after dilution with KBr by a weight factor of 10. IR spectra were recorded in a transmission mode with a resolution of 4 cm^{-1}.

The IR measurement of adsorbed pyridine was carried out using an in situ quartz cell (Fig. 11). The samples were evacuated at 473 K for 1 h and then exposed to pyridine vapor (2.7 kPa) followed by evacuation at the same temperature. After the sample was cooled to room temperature, the IR spectra were measured with a resolution of 4 cm^{-1}.

2.5. W-L_1 and W-L_3 edge XAFS measurement

W-L_1 (12.1 keV) and W-L_3 edge (10.2 keV) XAFS data were collected at the BL01B1 station of the Japan Synchrotron Radiation Research Institute. A Si(111) single crystal was used to obtain a monochromatic X-ray beam. Measurements were done in the quick mode. The ion chambers filled with N_2 and N_2(50%)/Ar(50%) were used for I_0 and I, respectively. The energy was calibrated using W foil. The wafer-form samples were pretreated at 673 K (calcined at 673–873 K) or 573 K (calcined at 573 K) under an N_2 flow. After the sample was cooled to room temperature, it was sealed in a polyethylene bag in a glove box. The data analysis was performed using the REX2000 Ver.2.0.4 program (Rigaku). Fourier transformation of $k^3\chi(k)$ data was performed in the k range of 20–150 nm^{-1} for the analysis of the W L_3-edge spectra.

2.6. TPD of ammonia

The acid property of catalysts derived from H_3PO_4–WO_3–Nb_2O_5 was measured by means of TPD of ammonia. The sample was evacuated at 673 K before measurement. As an exception, the sample calcined at 573 K was also pretreated at the same temperature. A total of 13.3 kPa of ammonia was equilibrated with the pretreated sample at 373 K. The TPD data were collected with a temperature ramping rate of 10 K min^{-1}. A mass spectrometer was used to measure the desorbed NH_3. In the measurement, $m/e = 16$ was monitored to analyze the desorbed NH_3. This mass number was used instead of $m/e = 17$ to prevent the interference caused by water.

Table 1
Data of the reaction between benzyl alcohol and anisole over various catalysts[a]

Catalyst	Benzyl alcohol conversion (%)	Benzyl-anisole yield (%)	Dibenzyl ether yield (%)	Material balance (%)
Nb_2O_5	0	0.2	0.1	102
WO_3	1.2	0.3	0.1	99
H_3PO_4(14 wt%)–Nb_2O_5	0	3.4	1.5	105
H_3PO_4(11 wt%)–WO_3	0	0.5	0.1	105
WO_3–Nb_2O_5	35	26.8	3.5	99
H_3PO_4–WO_3–Nb_2O_5	100	93.4	0.3	93
H_3PO_4–WO_3–Nb_2O_5[b]	100	94.0	0.3	94

[a] Reaction temperature, 353 K. The catalysts were calcined at 773 K during the preparation.
[b] Third run.

3. Results

3.1. Catalytic reaction

Data on the catalytic performance of H_3PO_4–WO_3–Nb_2O_5 and several other combinations of oxides are given in Table 1. Nb_2O_5, WO_3, H_3PO_4–WO_3, and H_3PO_4–Nb_2O_5 were substantially inactive in the reaction at 353 K. These catalysts were prepared by evacuating the respective precursor solutions ($(NH_4)_{10}W_{12}O_{41}$, niobic oxalate, phosphoric acid), followed by calcination at 773 K in air in a manner similar to the preparation of H_3PO_4–WO_3–Nb_2O_5. In contrast, 35% of the benzyl alcohol conversion was realized when using WO_3–Nb_2O_5 (40 wt% Nb_2O_5). H_3PO_4–WO_3–Nb_2O_5 exhibited 100% benzyl alcohol conversion, the highest conversion value among these oxides. On this catalyst, *ortho*- and *para*-substituted benzylanisole were obtained as products with 54% selectivity to *p*-benzylanisole, whereas *meta*-benzylanisole was not detected.

Subsequently, the H_3PO_4–WO_3–Nb_2O_5 catalysts with different amounts of H_3PO_4 were prepared, with the composition of Nb_2O_5 and WO_3 fixed at 40 and 60 wt%, respectively. This is because the optimum composition of WO_3–Nb_2O_5 for the reaction was determined to be 10–40 wt% Nb_2O_5 [17]. The prepared catalysts were subjected to the reaction at 333 K, and the composition of the catalyst was optimized. The highest activity was realized when the concentration of H_3PO_4 reached 8.6 wt% (54.8 wt% WO_3, 36.6 wt% Nb_2O_5), as shown in Fig. 1. Fig. 2 shows the dependence of benzylation activity on reaction temperature. The activity of H_3PO_4–WO_3–Nb_2O_5 appeared at 323 K, and 98% conversion was obtained at 343 K. At this temperature, the benzylanisole yield was 94%, indicating the high selectivity obtained with H_3PO_4–WO_3–Nb_2O_5. The conversion values and yields for H_3PO_4–WO_3–Nb_2O_5 were 4 times greater than those for montmorillonite-K10 clay treated with sulfuric acid, which was reported to be active for this kind of reaction [18]. The activity of H-beta zeolite ($Si/Al_2 = 20$, PQ Co.) was even lower than that of montmorillonite-K10 clay, as shown in Fig. 2.

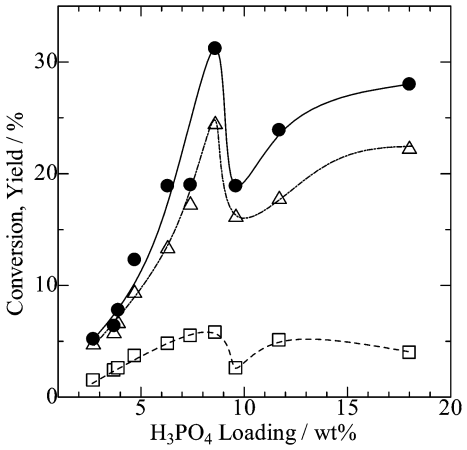

Fig. 1. (●) Conversion of benzyl alcohol, (△) yield of benzylanisole, and (□) dibenzyl ether plotted as a function of the concentration of H_3PO_4 present in H_3PO_4–WO_3–Nb_2O_5. The loading of Nb_2O_5 with respect to WO_3–Nb_2O_5 was fixed at 40 wt%. The catalysts were calcined at 773 K. Reaction temperature, 333 K; reaction time, 3 h.

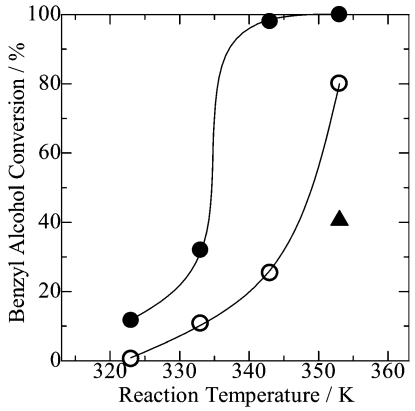

Fig. 2. Dependence of the conversion of benzyl alcohol on the reaction temperature. (●) H_3PO_4–WO_3–Nb_2O_5 calcined at 773 K, (○) montmorillonite-K10 clay treated with sulfuric acid, and (▲) H-beta zeolite ($Si/Al_2 = 20$).

Recycling of H_3PO_4–WO_3–Nb_2O_5 was attempted at 353 K by simply separating the catalyst by filtration followed by washing with anisole to remove products remaining from the first run. Further pretreatment was not done in the repeated reaction. As shown in Table 1, 100% conversion of benzyl alcohol was maintained after recycling three times. This implies that the deactivation of H_3PO_4–WO_3–Nb_2O_5 (calcined at 773 K) did not occur with repeated use of the catalyst. No further reaction occurred in the filtrated solution in the presence of residual benzyl alcohol, indicating that the catalytic reaction truly occurred over the solid catalyst. Such reusability of H_3PO_4–WO_3–Nb_2O_5 was confirmed only for the sample calcined at 773 K, as described later in this paper. As an experiment for comparison, HPW (HPW loading, 60 wt%) was impregnated on Nb_2O_5 (Wako Co.), followed by calcination at 773 K in air (denoted by HPW/Nb_2O_5).

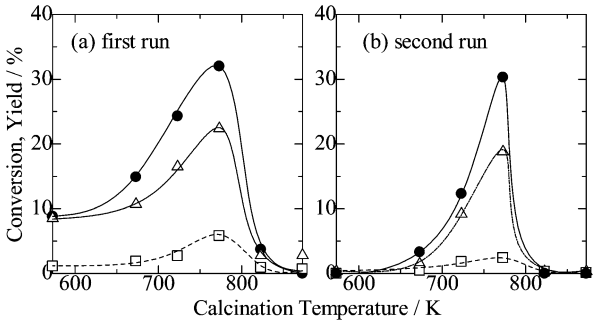

Fig. 3. Dependence of the (●) conversion of benzyl alcohol, (△) yield of benzylanisole, and (□) yield of dibenzyl ether on the calcination temperature of H_3PO_4–WO_3–Nb_2O_5. (a) First run and (b) second run. Reaction temperature, 333 K; reaction time, 3 h.

Although HPW/Nb_2O_5 exhibited high (42%) benzyl alcohol conversion in the first run at 333 K, conversion decreased to 8.9% in the second run, implying that recycling was not possible for the catalyst prepared by impregnation.

Fig. 3a shows the relationship between the catalytic activity of H_3PO_4–WO_3–Nb_2O_5 and the calcination temperature. The reaction was performed at 333 K. The conversion and yield of products increased with an increase in calcination temperature, and optimum activity was realized using the catalyst calcined at 773 K. Further increases in calcination temperature (above 823 K) caused activity to decline rapidly. In agreement with the decline in activity between 773 and 823 K, the color of the catalysts changed from white to green. The catalysts were separated by filtration, then subjected to the second run of the reaction (Fig. 3b). This figure shows that the activity of the catalysts calcined at 573–673 K was considerably reduced in the second run, but the catalyst calcined at 773 K maintained almost the same activity in the second run as in the first run. Consequently, the dependence of calcination temperature on the activity peaked sharply. These data demonstrate that catalytic activity and reusability were significantly sensitive to calcination temperature.

3.2. Structural analysis with IR, XRD, and XAFS

The structural change of H_3PO_4–WO_3–Nb_2O_5 prepared with varying calcination temperatures was investigated by means of IR spectroscopy, XRD, and XAFS. Fig. 4 shows the IR spectra of H_3PO_4–WO_3–Nb_2O_5 diluted with KBr 1:10 before measurements were obtained. Intense peaks appeared at 1080, 985, 889, and 820 cm^{-1} in the catalyst calcined at 673 K. The spectra closely agreed with the spectrum of authentic tungstophosphoric acid ($H_3PW_{12}O_{40}$). These peaks were attributed to the stretching vibrations of ν_{as}(P–O), ν_{as}(W=O), ν_{as}(W–O_c–W), and ν_{as}(W–O_e–W), respectively [19,20]. Thus, the formation of HPA species similar to HPW was inferred from the IR data. The intensity of the peaks ascribed to HPA decreased markedly after the benzylation reaction with the catalyst calcined at 673 K. This finding suggests that the deactivation of the second run was caused by the dissolution of HPA in the solution, be-

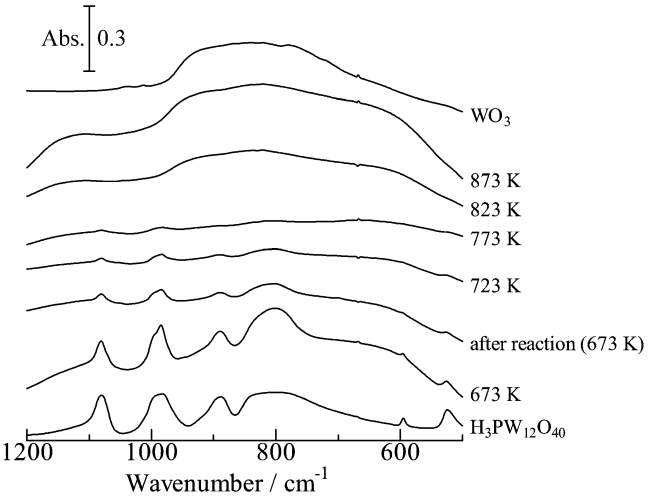

Fig. 4. IR spectra of H_3PO_4–WO_3–Nb_2O_5 calcined at different temperatures.

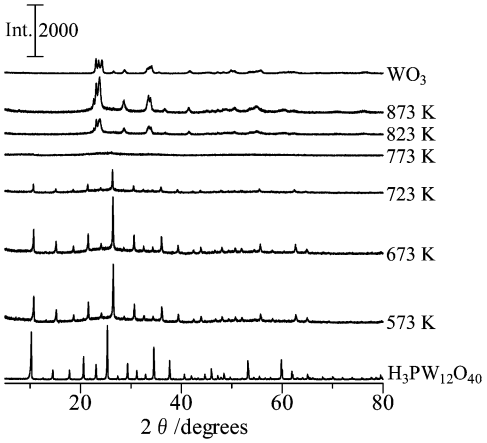

Fig. 5. Powder XRD patterns of H_3PO_4–WO_3–Nb_2O_5 calcined at different temperatures.

cause the active species of the catalyst calcined at 573–673 K was HPA. The intensity of the absorption bands of HPA decreased, accompanied by a raise in the calcination temperature, and only small peaks remained in the sample calcined at 773 K. These peaks diminished after calcination above 823 K, at which point the spectra became similar to the spectrum of WO_3. The change in the IR spectrum suggested that HPA was completely decomposed in the temperature range 773–823 K.

Fig. 5 displays the XRD patterns of H_3PO_4–WO_3–Nb_2O_5 calcined at different temperatures. Intense diffraction peaks appeared in the catalysts calcined at 573 and 673 K. The patterns were similar to the pattern of HPW dehydrated at 373 K, but with peak positions shifted slightly to the greater angle. The molar ratio of W to Nb present in HPA was analyzed to investigate the reason for the shift in XRD patterns. For this purpose, H_3PO_4–WO_3–Nb_2O_5 calcined at 673 K was washed thoroughly with deionized water to dissolve HPA, and the filtered solution was then analyzed using the ICP method. The atomic ratio of W to Nb determined by

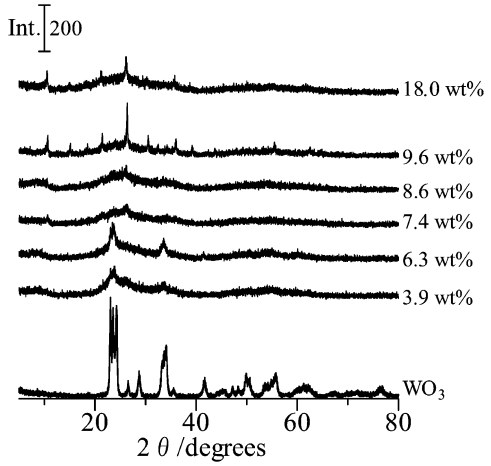

Fig. 6. Powder XRD patterns of the H_3PO_4–WO_3–Nb_2O_5 with different loading of H_3PO_4. Calcination was carried out at 773 K.

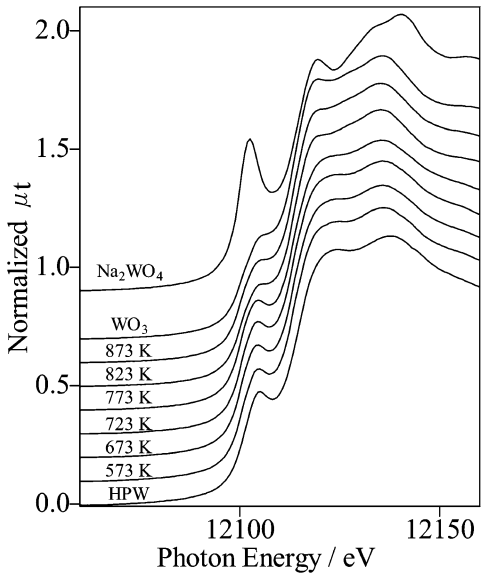

Fig. 7. W-L_1 XANES of H_3PO_4–WO_3–Nb_2O_5 calcined at different temperatures, HPW, WO_3 and Na_2WO_4 (dehydrated at 423 K).

analyzing the filtrate was 10:1, suggesting that one tungsten atom present in HPW was substituted by a niobium atom in HPA. It is possible that the partial substitution of W with Nb caused the slight shift in the peaks obtained from XRD patterns. With further temperature increases, the intensity of the diffractions decreased at 723 K and completely disappeared at 773 K. New diffraction peaks then emerged in the samples calcined at 823 and 873 K that can be assigned to WO_3, as indicated from a comparison with that of authentic WO_3. The change in the XRD patterns indicates that the initially formed HPA began to decompose at 723 K and that complete transformation occurred between 773 and 823 K. Thus the temperature at which the transformation occurred closely agreed with that found in the IR spectra. In the XRD patterns, no diffractions due to the crystalline Nb_2O_5 appeared in the samples, suggesting the presence of amorphous Nb_2O_5. It seems likely that the amorphous Nb_2O_5 functioned as a support to disperse HPA and its derivatives.

Fig. 6 shows the XRD patterns for H_3PO_4–WO_3–Nb_2O_5 with a different loading of H_3PO_4, which was calcined at 773 K. In these samples, the loading of Nb_2O_5 with respect to WO_3–Nb_2O_5 was fixed at 40 wt%. Broad diffraction peaks ascribed to WO_3 appeared for H_3PO_4–WO_3–Nb_2O_5 with an H_3PO_4 loading of <6.3 wt%, suggesting that the total decomposition of HPA took place on the Nb_2O_5 support. In contrast, a number of sharp diffractions assigned to the HPA were observed for H_3PO_4–WO_3–Nb_2O_5 with an H_3PO_4 loading of >9.6 wt%, implying that the Keggin structure of HPA was retained. In contrast, no distinctive diffractions appeared on the sample with an intermediate loading of H_3PO_4 (7.4 and 8.6 wt%), which exhibited the highest activity in the reaction, as shown in Fig. 1.

Fig. 7 shows the W-L_1 XANES spectra of H_3PO_4–WO_3–Nb_2O_5 calcined at different temperatures, HPW, WO_3, and Na_2WO_4. In these spectra, a pre-edge peak appeared at 12105 eV. This pre-edge peak is due to the electronic transition from 2s to 5d. It is known that the intensity of the pre-edge peak is sensitive to the local symmetry around the W atoms; in other words, the intensity of the pre-edge peak is the largest in the tetrahedral coordination and becomes smaller in the octahedral environment [21]. The intensity of the peak of the W-L_1 XANES spectra of H_3PO_4–WO_3–Nb_2O_5 did not change between 573 and 773 K, implying that the local symmetry around W was retained up to 773 K. However, the intensity of the pre-edge peak decreased above 823 K, and the shape became similar to that of WO_3, which had distorted octahedral units. But the spectra of H_3PO_4–WO_3–Nb_2O_5 were completely different from that of Na_2WO_4, which has a tetrahedral symmetry.

Fig. 8 shows the W-L_3 EXAFS $k^3\chi(k)$ and their Fourier transforms of H_3PO_4–WO_3–Nb_2O_5 calcined at different temperatures, HPW and WO_3. In the $k^3\chi(k)$ spectra, rapid oscillations due to the W–O–W bonds of the Keggin structure appeared at 70–150 nm^{-1} in the spectra calcined at 573–723 K, which was clearly seen in the spectrum of HPW [22]. The oscillations weakened notably at 773 K and finally disappeared at 823 K, where the spectrum was close to that of WO_3. In the Fourier transforms of the spectra for the H_3PO_4–WO_3–Nb_2O_5 calcined at 573 and 673 K, split peaks due to W–O and W=O bonds appeared at 0.1–0.18 nm. In contrast, W–O–W bonds due to the Keggin structure appeared at 0.3–0.4 nm (phase shift uncorrected). The intensity of the W–O–W peak decreased at 773 K and disappeared at 823 K, as was seen previously from the Fourier transforms. The change in $k^3\chi(k)$ as well as in the Fourier transforms of the W-L_3 edge spectra suggested that partial decomposition of the Keggin structure occurred at 773 K and decomposition was completed at 823 K. The observation was in agreement with the XRD and IR data given earlier.

The IR, XRD, and XAFS data confirmed that at the optimum calcination temperature (773 K) and loading of H_3PO_4 (8.6 wt%), the active species for the catalytic reaction corre-

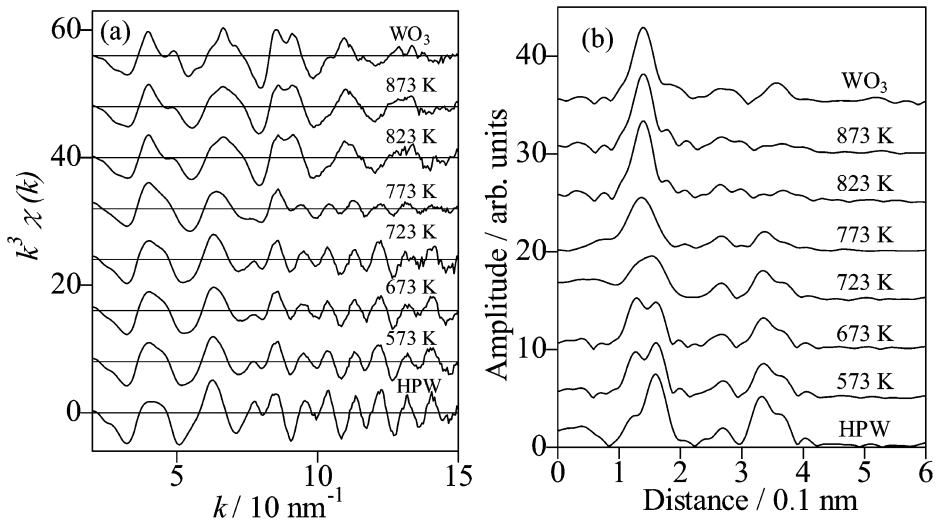

Fig. 8. W-L_3 EXAFS (a) $k^3\chi(k)$ and (b) their Fourier transforms of H_3PO_4–WO_3–Nb_2O_5 calcined at different temperatures, HPW and WO_3. Fourier transform range, 20–150 nm^{-1}.

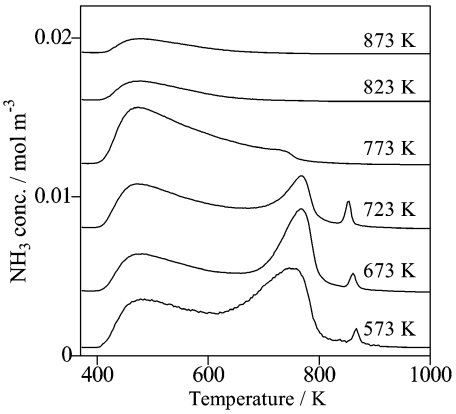

Fig. 9. NH_3 TPD of H_3PO_4–WO_3–Nb_2O_5 calcined at different temperatures.

sponded to the intermediate compound formed during the decomposition of HPA to yield crystalline WO_3. Although the HPA generated at 573–673 K itself exhibited low activity and severe solubility, the catalyst calcined at 773 K had superior characteristics, with high activity and facile reusability.

3.3. Acid properties

The acid properties of H_3PO_4–WO_3–Nb_2O_5 were examined by the NH_3 TPD method and IR spectra of adsorbed pyridine. Fig. 9 shows the NH_3 TPD of H_3PO_4–WO_3–Nb_2O_5 calcined at different temperatures. In the spectra of H_3PO_4–WO_3–Nb_2O_5 calcined at 573–723 K, desorption peaks appeared at 475 and 750 K, in addition to the sharp peaks at 860 K. It is possible that the peak at 750 K could be ascribed to the desorption from HPA accompanied by the decomposition of HPA, because the temperature agreed with that of the decomposition of HPW. Desorption from HPA decreased when the calcination temperature increased up to 773 K and diminished completely for the sample calcined above 823 K. In contrast, the broad peak at 475 K may be attributed to desorption from the acid sites generated on the Nb_2O_5 support and the partially decomposed HPA, as described later in this paper. The intensity of the weak desorption peak increased up to 773 K, followed by a marked decrease above 823 K. The sharp peak that emerged at 860 K was considered to have possibly originated from the fragment of CO_2, not from NH_3. This is because such desorption was not observed in the spectra of $m/e = 17$, whereas the desorption of CO_2 was detected at the same temperature (860 K). Therefore, the desorption at 860 K was neglected in further calculations of the desorbed amount of NH_3.

Fig. 10 shows the amount and concentration of acid sites present in H_3PO_4–WO_3–Nb_2O_5. In the calculation, the NH_3 TPD spectra were deconvoluted into desorptions from weak (475 K) and strong (750 K) acid sites. The concentration of the acid sites was determined on the basis of the NH_3 TPD and BET surface area. The surface area of H_3PO_4–WO_3–Nb_2O_5 decreased in the order of calcination temperature, that is, 573 K (105 $m^2\,g^{-1}$) > 673 K (96 $m^2\,g^{-1}$) > 723 K (77 $m^2\,g^{-1}$) > 773 K (58 $m^2\,g^{-1}$) > 823 K (36 $m^2\,g^{-1}$) > 873 K (25 $m^2\,g^{-1}$). The acid concentration of strong acid sites decreased from 573 to 773 K and diminished at 823 K. It is possible that the decomposition of HPA was responsible for the reduction in the strong acidity, because the signal due to HPA reduced at the same temperature region in the IR and XRD methods. However, the concentration of weak acid sites increased up to 773 K. This change corresponded with the decrease in the acid concentration of HPA observed in the same temperature range. The simultaneous change in acid concentration suggests that the partially decomposed HPA was transformed into the weak acid sites. Raising the temperature above 823 K caused a rapid reduction in the concentration of acidity. This change coincided with the total decomposition of HPA to form crystalline WO_3, as indicated by XRD patterns.

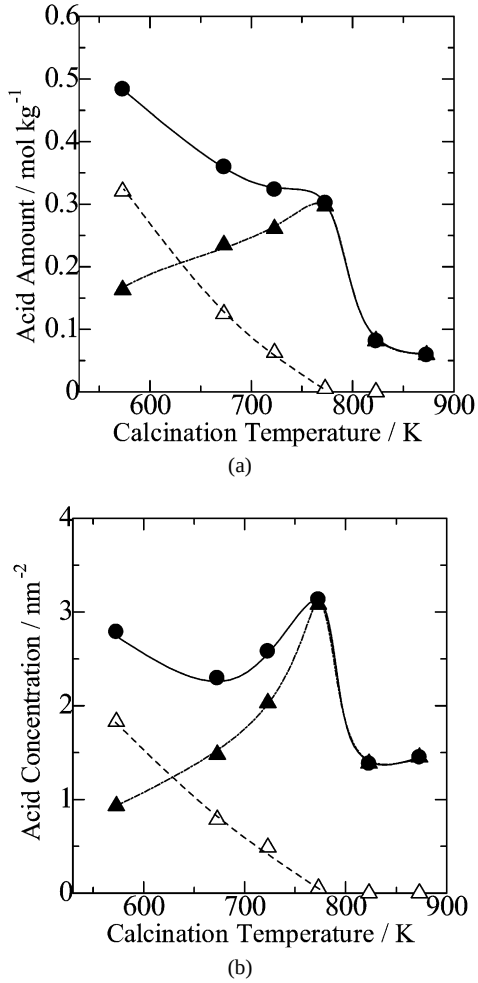

Fig. 10. Dependence of the (a) acid amount and (b) acid concentration of H_3PO_4–WO_3–Nb_2O_5 on the calcination temperature determined based on the NH_3 TPD. (●) Total acid amount, (▲) weak acid, and (△) strong acid (HPA).

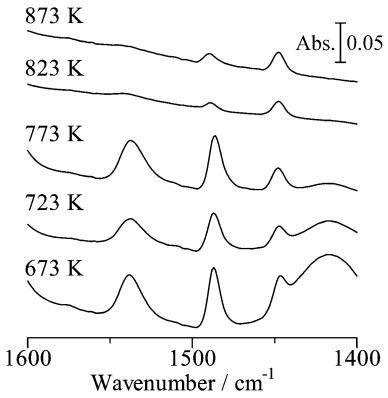

Fig. 11. IR spectra of the adsorbed pyridine over H_3PO_4–WO_3–Nb_2O_5 calcined at different temperatures.

Fig. 11 shows the IR spectra of adsorbed pyridine over H_3PO_4–WO_3–Nb_2O_5 calcined at different temperatures. Pyridine adsorbed on the Brønsted and Lewis acid sites appeared at 1538 and 1448 cm^{-1}, respectively. The broad band observed at 1417 cm^{-1} on the calcined samples at 673 and 723 K may be assigned to the water of crystallization present in HPA, taking into consideration that crystalline HPA was found at the corresponding temperature range in the XRD patterns (Fig. 5). As Fig. 11 shows, the intensity of pyridine adsorbed on the Brønsted acid sites was significantly greater than that absorbed on the Lewis acid sites when the sample was calcined at 673–773 K, whereas the intensity of the Brønsted acidity decreased significantly on the samples calcined above 823 K, due to the formation of WO_3.

4. Discussion

Comparison of the catalytic activity using Nb_2O_5, WO_3, H_3PO_4–WO_3, and H_3PO_4–Nb_2O_5 revealed that the combination of H_3PO_4–WO_3–Nb_2O_5 exhibited high activity in the benzylation of anisole. The activity of H_3PO_4–WO_3–Nb_2O_5 was superior to that of montmorillonite-K10 clay treated with sulfuric acid or H-beta zeolite. In addition, H_3PO_4–WO_3–Nb_2O_5 exhibited the excellent characteristic of being recyclable simply by filtration followed by washing of the catalyst. However, the catalytic performance and reusability of H_3PO_4–WO_3–Nb_2O_5 was quite sensitive to the calcination temperature in the preparation step. In other words, although the H_3PO_4–WO_3–Nb_2O_5 calcined at 773 K exhibited high activity and reusability during the reaction, the catalysts calcined at 573–723 K showed lower activity and poor reusability, due to the dissolution of HPA. In contrast, the H_3PO_4–WO_3–Nb_2O_5 calcined above 823 K exhibited limited activity because of the total decomposition of HPA. Hence this can be interpreted as indicating that the temperature of 773 K was an important factor in generating the active and insoluble species.

The disintegration of HPW was reported to have progressed through the dehydration of constitutional or structural water at 333–623 K, followed by total decomposition to form WO_3 and P_2O_5 at 823 K [23]. The IR and XRD measurements revealed that the active species generated in the H_3PO_4–WO_3–Nb_2O_5 calcined at 773 K corresponded to the intermediate phase of HPA to finally produce WO_3 and P_2O_5 (not detected), because the temperature of 773 K was slightly lower than that at which HPA decomposed completely (823 K). In agreement with this finding, the generation of weak acid sites was observed in the sample calcined at 773 K, as indicated by NH_3 TPD. The dependence of the acid concentration and the activity on calcination temperature were very similar (Figs. 3 and 10). Therefore, the novel acid sites present in the intermediate species that were insoluble in the solvent could be attributed to the active sites for the reaction. Here the “novel acid sites” represent the relatively weak acidity generated accompanied by a rise in the calcination temperature of H_3PO_4–WO_3–Nb_2O_5 with a maximum at 773 K, as shown in Fig. 10 (▲) (the desorption of NH_3 with the maximum at 473 K). Brønsted acid sites dominated the intermediate species generated at 773 K as characterized by the IR spectra of adsorbed pyridine. It

is possible that the weak Brønsted acidity acted as an active site for the formation of benzyl cation from benzyl alcohol in the course of Friedel–Crafts alkylation, resulting in high activity. Although it has been recognized that the decomposition of HPA gave rise to the decrease in acid concentration, the data from NH_3 TPD (Figs. 9 and 10) indicated the formation of a novel acid site in the course of HPA decomposition. It has been reported that the Keggin of HPA transforms to yield a unique type of oxide above 673 K [24]. Mestl et al. [25] proposed that the defective Keggin structure is formed in the initial disintegration of $H_4PVMo_{11}O_{40}$ (Keggin structure), and that the defective structure then disintegrates to Mo_3O_{13} triads (fragment of HPA) before the formation of crystalline MoO_3. The thermal decomposition of HPW has been proposed to occur through the formation of $HPW_{12}O_{39}$ due to dehydration, followed by the formation of WO_3, PO_x, and H_2O [26]. In light of the previous reports, it is most likely that the defective Keggin structure or fragment of HPA generated at 773 K on the surface of the Nb_2O_5 support is due to the active and insoluble species, although the precise decomposition resulting in WO_3, PO_x, and H_2O remains unclear. In agreement with this hypothesis, the partially decomposed HPA was observed in the EXAFS W-L_3 edge spectra, as shown in Fig. 8. In a manner similar to the present study, in an investigation of WO_3/SiO_2 for the selective oxidation of cyclopentene to glutaraldehyde, Xia et al. [27] proposed that the partially decomposed Keggin-type structure was involved in the reaction. Further investigation is needed to reveal the structure of the intermediate species generated at 773 K.

5. Conclusions

H_3PO_4–WO_3–Nb_2O_5-derived catalyst prepared with the evacuation of the mixed solution of phosphoric acid, niobic oxalate, and $(NH_4)_{10}W_{12}O_{41}$ exhibited excellent activity in the reaction between benzyl alcohol and anisole. The catalytic performance and reusability of H_3PO_4–WO_3–Nb_2O_5 were sensitive to the calcination temperature to a considerable extent, and a temperature of 773 K was found to be the optimum condition. In other words, the catalyst calcined at 773 K exhibited the highest activity and could be reused merely by filtration after the reaction. In the sample calcined at 773 K, formation of the intermediate species in the course of HPA decomposition was detected through IR and XRD measurements. On the basis of the W-L_3 EXAFS and W-L_1 XANES analysis, the intermediate species was ascribed to the partially decomposed HPA, although it retained the same local symmetry of W atoms as HPA. The change in the acid properties could be detected through the NH_3 TPD spectra. Accompanied by HPA decomposition, the acidity due to HPA decreased and almost diminished at 773 K. Alternatively, relatively weak acid sites (from the desorption of NH_3, with a maximum at 473 K) developed. The Brønsted acidity was dominant for the catalyst calcined at 773 K, as characterized by the IR spectra of adsorbed pyridine. The relatively weak acidity was considered to indicate the presence of the novel acid site in the fragment of HPA, considering that concentration peaked at a pretreatment temperature of 773 K. This temperature closely agreed with that for the optimum condition for catalysis. Therefore, the novel acid sites with Brønsted acid characteristics were ascribed to the active sites for the benzylation of anisole. It is possible that the Brønsted acidity functioned as the catalyst for the formation of benzyl cation ($C_6H_5CH_2^+$), which attacked the anisole ring in course of the Friedel–Crafts alkylation.

Acknowledgment

This work was supported by a Grant-in-Aid for Scientific Research (KAKENHI) in Priority Area “Molecular Nano Dynamics” from the Japanese Ministry of Education, Culture, Sports, Science, and Technology.

References

[1] M. Misono, Catal. Rev. Sci. Eng. 29 (1987) 269.
[2] Y. Izumi, K. Urabe, Zeolite, Clay, and Heteropoly Acid in Organic Reactions, VCH, Tokyo, 1992.
[3] I.V. Kozhevnikov, Appl. Catal. A 256 (2003) 3.
[4] M.N. Timofeeva, Appl. Catal. A 256 (2003) 19.
[5] Y. Izumi, M. Ono, M. Kitagawa, M. Yoshida, K. Urabe, Micropor. Mater. 5 (1995) 255.
[6] I.V. Kozhevnikov, Catal. Rev. Sci. Eng. 37 (1995) 311.
[7] T. Okuhara, Catal. Today 73 (2002) 167.
[8] M. Misono, Stud. Surf. Sci. Catal. 75 (1993) 69.
[9] S.R. Mukai, L. Lin, T. Masuda, K. Hashimoto, Chem. Eng. Sci. 56 (2001) 799.
[10] B. Sulikowski, J. Haber, A. Kubacka, K. Pamin, Z. Olejniczak, J. Ptaszyński, Catal. Lett. 39 (1996) 27.
[11] P.A. Jalil, A.A. Al-Arfaj, A.A. Al-Amer, J. Beltramini, S.A. Barri, Appl. Catal. A 207 (2001) 159.
[12] Á. Molnár, C. Keresszegi, B. Török, Appl. Catal. A 189 (1999) 217.
[13] B. Bachiller-Baeza, J.A. Anderson, J. Catal. 212 (2002) 231.
[14] S. Narayanan, K.V.V.S.B.S.R. Murthy, Appl. Catal. A 213 (2001) 273.
[15] P. Laszlo, Science 235 (1987) 1473.
[16] M.P. Hart, D.R. Brown, J. Mol. Catal. A 212 (2004) 315.
[17] K. Yamashita, M. Hirano, K. Okumura, M. Niwa, in preparation.
[18] T. Cseri, S. Bekassy, F. Figueras, E. Cseke, L.-C. de Menorval, R. Dutartre, Appl. Catal. A 132 (1995) 141.
[19] T. Okuhara, N. Mizuno, M. Misono, Adv. Catal. 41 (1996) 113.
[20] M. Hashimoto, G. Koyano, N. Mizuno, J. Phys. Chem. B 108 (2003) 12368.
[21] A. Kuzmin, J. Purans, J. Phys.: Condens. Matter 5 (1993) 9423.
[22] T. Miyanaga, N. Matsubayashi, T. Fukumoto, K. Yokoi, I. Watanabe, K. Murata, S. Ikeda, Chem. Lett. (1988) 487.
[23] P.A. Jalil, M. Faiz, N. Tabet, N.M. Hamdan, Z. Hussan, J. Catal. 217 (2003) 292.
[24] E.M. Serwicka, C.P. Grey, Colloids Surf. 45 (1990) 69.
[25] G. Mestl, T. Ilkenhans, D. Spielbauer, M. Dieterle, O. Timpe, J. Kröhnert, F. Jentoft, H. Knözinger, R. Schlögl, Appl. Catal. A 210 (2001) 13.
[26] B.W.L. Southward, J.S. Vaughan, C.T. O’Connor, J. Catal. 153 (1995) 293.
[27] X. Xia, R. Jin, Y. He, J.-F. Deng, H. Li, Appl. Surf. Sci. 165 (2000) 255.